Journal of Applied Polymer Science

Reduced sedimentation of barium titanate nanoparticles in poly(vinylidene fluoride) films during solution casting by surface modification

Rongyan Zhao, Jun Zhao, Lina Wang, Zhi-Min Dang
Department of Polymer Science and Engineering, School of Chemistry and Biological Engineering, University of Science and Technology Beijing, Beijing 100083, People's Republic of China
Correspondence to: Z.-M. Dang (E-mail: dangzm@ustb.edu.cn)

ABSTRACT: Reduced sedimentation of barium titanate ($BaTiO_3$, BT) nanoparticles during solution casting to prepare the BT/poly(vinylidene fluoride) (PVDF) films is systematically investigated by surface modification of the BT nanoparticles. The surface of BT nanoparticles is hydroxylated by hydrogen peroxide (H_2O_2) or aminated by γ-aminopropyl triethoxysilane (γ-APS). It is found that the compatibility between the fillers and polymer matrix is remarkably improved by such surface treatments. As a result, the agglomeration and sedimentation of BT nanoparticles in the BT/PVDF composite films are significantly reduced, which is supported by morphology observation. Better dielectric properties such as higher dielectric constant, higher breakdown strength, and lower dielectric loss are also obtained for the composite films with surface-modified fillers than those with raw fillers. © 2015 Wiley Periodicals, Inc. J. Appl. Polym. Sci. **2015**, *132*, 42662.

KEYWORDS: composites; dielectric properties; films

Received 11 February 2015; accepted 24 June 2015
DOI: 10.1002/app.42662

INTRODUCTION

Polymer films used as dielectric materials are characterized by their excellent properties such as high insulating resistance, low dielectric loss, high breakdown strength, good mechanical properties, perfect processability, and low cost, which are completely different from dielectric ceramics.[1] The most widely used dielectric polymers are polypropylene (PP), polyethylene (PE), polystyrene (PS), poly(methyl methacrylate) (PMMA), poly(vinylidene fluoride) (PVDF), epoxy resin, and polyimide (PI).[2–14] However, most of them have low dielectric constant (ε), which limits their applications as energy-storage dielectric materials in capacitors, piezo- and pyroelectric sensors, and field-activated actuators. To increase the ε of polymer materials, a variety of methods have been proposed in the past decades.[15,16] Among them, the most frequently employed one is to prepare polymer composites by adding fillers with high ε or high electrical conductivity (σ) into the polymer matrix. High-ε fillers are mainly ceramics such as $BaTiO_3$ (BT), $SrTiO_3$, TiO_2, and $CaCuTiO_3$, while high-σ fillers include metals such as Ag and Al, or carbon materials such as carbon black (CB), graphite, carbon fiber (CF), carbon nanotube (CNT), and grapheme are often used to increase the dielectric permittivity of polymers by means of percolation effect.[17–25]

A great challenge during the preparation of such polymer nanocomposite films is how to homogeneously disperse fillers in the polymer matrix, which is critical to the final properties of films.[20,22] Most nano-size fillers have strong tendency to agglomerate due to the small size and high surface-to-volume ratio.[26] Besides, vertical gradient of fillers' distribution is often observed due to the gravity, which causes big discrepancy from the upper to lower surfaces. This sedimentation problem is usually more serious for solvent casting processing than for melt blending due to the lower viscosity of the solution than that of the melt. Obviously, this phenomenon will deteriorate the final properties of the nanocomposite films.

This work will focus on how to solve this sedimentation problem. BT nanoparticles and PVDF are chosen as the fillers and the matrix, respectively. The surface of BT nanoparticles will be hydroxylated by hydrogen peroxide (H_2O_2) or aminated by γ-aminopropyl triethoxysilane (γ-APS). Then agglomeration and sedimentation of the surface-modified fillers during solution casting with *N*,*N*-dimethyl formamide (DMF) as solvent will be checked and compared with the raw fillers. The effect of such surface treatments on the dielectric properties will also be investigated.

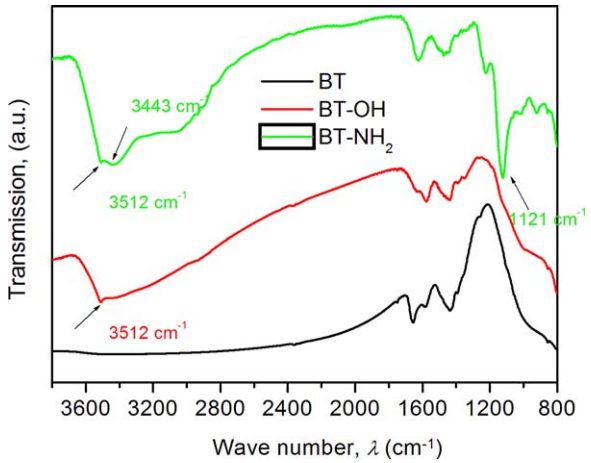

Figure 1. FTIR spectra of the raw and modified BT nanoparticles. All the curves are shifted vertically for clarity. [Color figure can be viewed in the online issue, which is available at wileyonlinelibrary.com.]

EXPERIMENTAL

Materials

PVDF (type FR901) pellets with density of 1.78 g cm^{-3}, molecular weight is 300,000 and melt flow index of 26 g $(10\ min)^{-1}$ were purchased from Shanghai 3F New Materials Company (China). BT nanoparticles (99.9%, trace metals basis) with diameter of 100–200 nm, and density of 6.0 g cm^{-3} were purchased from Aladdin Industrial Corporation (China). H_2O_2 (30 wt %, AR), γ-APS (CP), DMF (AR), and toluene (AR) were purchased from National Medicine Group Chemical Reagent (China), Beijing Tranche Reagent Factory (China), Beijing Chemical Plant (China), and Beijing Blue Yi Chemical Products, respectively.

Surface Hydroxylation of BT Nanoparticles

BT nanoparticles were hydroxylated according to a method given in literature.[27] 15 g BT nanoparticles and 80 mL aqueous solution of H_2O_2 (30 wt %) were added into a 100 mL flask. Then the mixture was sonicated at room temperature for 30 min and refluxed at 105°C for 4 h. Afterwards, the nanoparticles were recovered by centrifugation at 10^3 rpm for 10 min and washed with deionized water twice. Finally, the obtained hydroxylated BT nanoparticles were dried up under vacuum at 80°C for 12 h.

Surface Amination of BT Nanoparticles

BT nanoparticles were aminated according to a method given in the literature.[28] 10 g BT-OH nanoparticles and 80 mL toluene were added into a 100 mL flask and then sonicated at room temperature for 30 min. Subsequently, 5 g γ-APS was added and the mixture was heated up to 80°C and kept isothermal for 24 h under a nitrogen (N_2) atmosphere. Afterwards, the nanoparticles were recovered by centrifugation at 10^3 rpm for 10 min and washed with toluene twice. Finally, the obtained aminated BT nanoparticles were dried up under vacuum at 80°C for 12 h.

Preparation of BT/PVDF Nanocomposites

A given amount of the raw or surface-modified BT nanoparticles was ultrasonically dispersed in DMF for 0.5 h. PVDF pellets were dried completely in a vacuum oven at 80°C

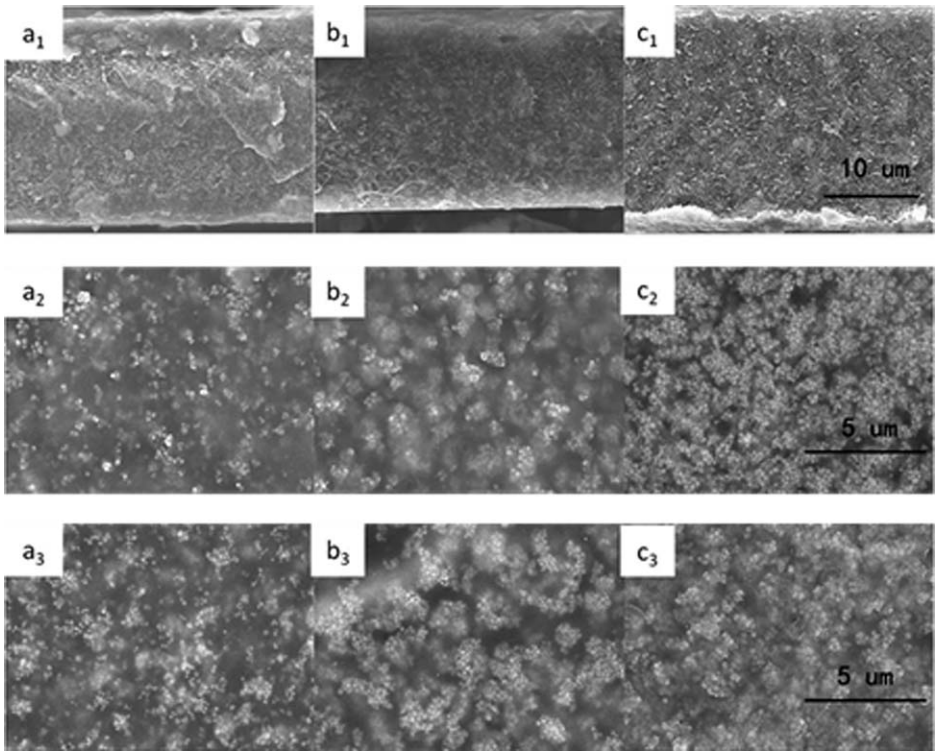

Figure 2. SEM micrographs of the cross-section (a1, b1, c1), upper surface (a2, b2, c2), and lower surface (a3, b3, c3) of the BT/PVDF nanocomposite films with various fvBT of 10.0 vol % (a), 20.0 vol % (b), and 30.0 vol % (c) raw BT nanoparticles, respectively.

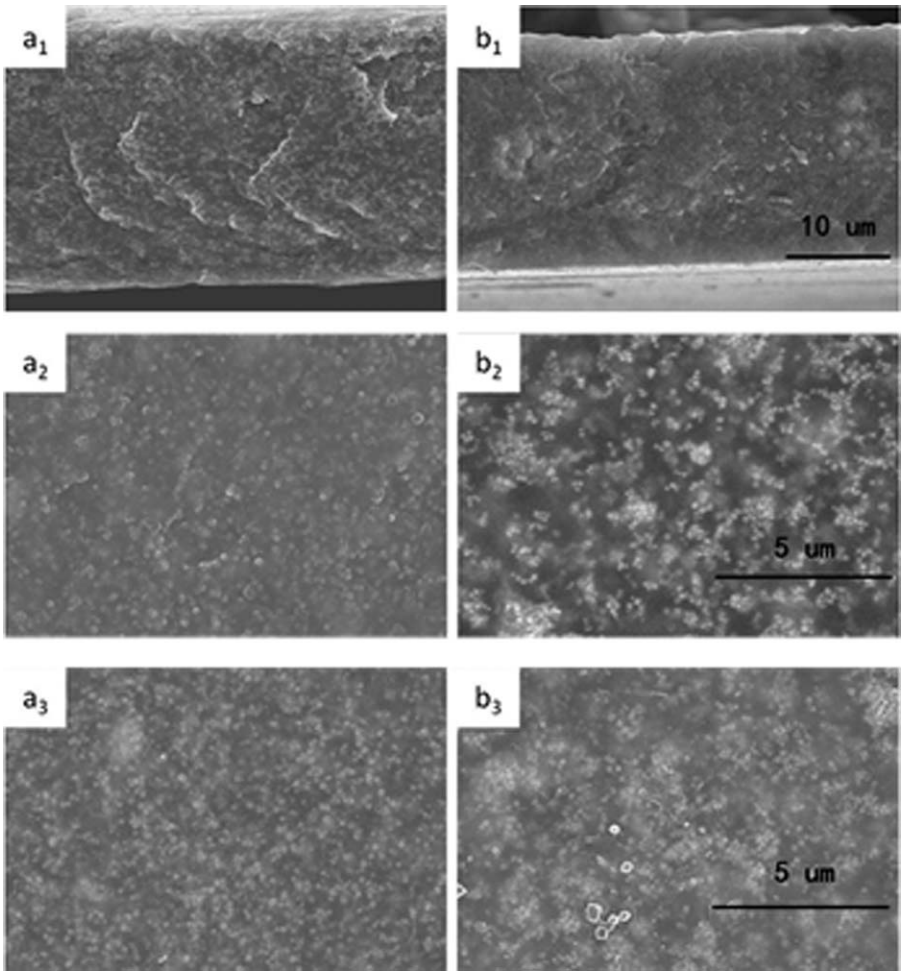

Figure 3. SEM micrographs of cross-section (a1, b1), upper surface (a2, b2), and lower surface (a3, b3) of PVDF nanocomposite films with fvBT of 20 vol % hydroxylated (a) and aminated (b) BT nanoparticles, respectively.

overnight before they were dissolved in DMF under mechanical stirring at 70°C for 1 h. Then the BT suspension was added to the PVDF solution and the mixture was further stirred at 70°C for 2 h. Afterwards, the mixture was casted on a clean glass plate and dried up in an oven at 80°C for 6 h. The mass fraction of PVDF in the solution was fixed at 20 wt % when preparing the nanocomposites with various volume fractions of BT. The thickness of the final dry films was set to be ca. 10 μm for the convenience of comparison. A similar method of preparing the nanocomposite films was also used in the literature.[29,30]

Fourier Transform Infrared (FTIR) Spectroscopy

The chemical structure of the BT and the modified-BT were characterized by the KBr disc method with a Fourier-transform infrared (FT-IR) spectrometer (Thermo Nicolet 6700) over the wavelength range of 3500-500 cm^{-1} with an interval of 2 cm^{-1} and repeat times of 15.

Scanning Electron Microscopy (SEM) Observation.

The nanocomposite samples were first fractured in liquid nitrogen before the fractured surfaces were sputtered with gold. Then the morphology observation was carried out on an S4700 SEM (Hitachi, Japan) running at an accelerating voltage of 20 kV.

Dielectric Measurements

For the dielectric measurements, the nanocomposite films prepared above were cut into circles with an area of ca. 1 cm^2. Both sides of the films were coated with silver as electrodes. The dielectric measurements were carried out on an Agilent 4294 Impedance Analyzer (Agilent Technologies, USA) at room temperature over the frequency range of 10^2-10^6 Hz.

Differential Scanning Calorimetry (DSC) Measurements

DSC measurements were performed on a DSC-60 (Shimadzu, Japan) in nitrogen atmosphere. The temperature and enthalpy calibration was made with indium as a standard. The samples of 5–10 mg were dried in a vacuum oven before they were sealed in aluminum crucibles. The samples were first heated to 220°C and kept isothermal for 3 min to eliminate the complex thermal history. Then they were cooled to 30°C at 10 K min^{-1} and kept isothermal for 3 min. Subsequently, they were heated to 220°C again at 10 K min^{-1}. Both the first cooling and second heating were recorded for analysis.

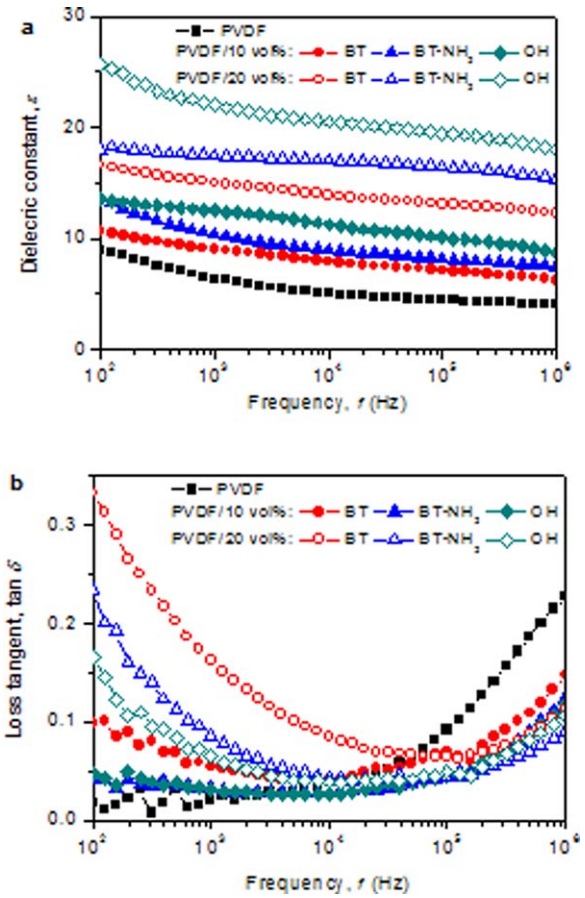

Figure 4. Frequency dependence of ε(a) and tanδ (b) at room temperature of the pure PVDF and PVDF nanocomposite films with various contents of the raw or modified BT nanoparticles. [Color figure can be viewed in the online issue, which is available at wileyonlinelibrary.com.]

Breakdown Strength Measurements

The electrical breakdown tests were performed on a high-voltage instrument (CS2674A, Nanjing Changsheng Instrument) with 25 mm diameter spherical electrodes. During the test, the applied voltage was increased rapidly with a rate of 2 kV s^{-1} till the samples were broken down. All the measurements were made on five different film samples. The breakdown strengths were averaged over nine measurements on each sample.

RESULTS AND DISCUSSION

Figure 1 presents the FTIR spectra of the raw BT, hydroxylated BT (BT-OH), and aminated BT (BT-NH_2) nanoparticles. The peak at ca. 3512 cm^{-1} for BT-OH can be associated with the stretching of O—H, which indicates successful hydroxylation of BT nanoparticles. The peaks at ca. 3512 cm^{-1} and 3443 cm^{-1} for BT-NH_2 can be assigned to the stretching of N—H, and the peak at 1121 cm^{-1} can be assigned to the stretching of C—N, which indicates successful amination of the fillers. For the raw BT, there is no peak appearing in this range of wavelength. This is because that there are some residual groups on the surface of BT particles which can react with H_2O_2 and KH550. The group of —OH might be valuable to polarization and make a strong contribution to the dielectric permittivity of composite films.

Figure 2 shows the SEM images of the fractured cross-section, upper surface, and lower surface of the PVDF nanocomposites with various volume fractions of BT nanoparticles (f_v^{BT}). As can be clearly seen, the extent of agglomeration and sedimentation of BT nanoparticles in the PVDF matrix is obviously different with the content of fillers. For the f_v^{BT} of 10.0 vol %, although the vertical gradient of the filler distribution is not clearly visible in the cross-section, there is already clear discrepancy between the upper surface and the lower surface: the former has fewer fillers than the latter [see Figure 2(a)]. For the f_v^{BT} of 20.0 vol %, even clearer discrepancy between the upper surface and the lower surface can be seen and somehow clear vertical gradient of filler distribution can be seen [see Figure 2(b)]. For the f_v^{BT} of 30.0 vol %, both the vertical gradient of filler distribution and the discrepancy between the two surfaces are highly visible [see Figure 2(c)]. Therefore, the extent of agglomeration and sedimentation of fillers in the polymer matrix increases with increasing content of fillers.

Figure 3 presents the SEM micrographs of the cross-section, upper surface, and lower surface of BT-OH/PVDF and BT-NH_2/PVDF nanocomposite films with f_v^{BT} of 20 vol %. Compared with the raw BT/PVDF nanocomposite films with the same filler content as shown in Figure 2(b), the modified BT/PVDF nanocomposites show much less distinct vertical gradient of the filler

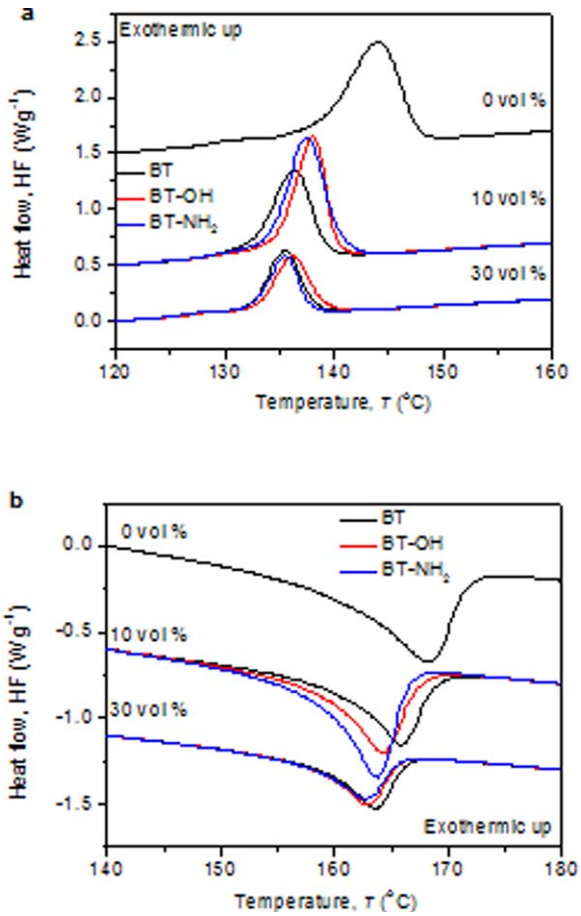

Figure 5. DSC HF traces of PVDF and BT/PVDF nanocomposite films in the cooling (a) and the second heating (b). [Color figure can be viewed in the online issue, which is available at wileyonlinelibrary.com.]

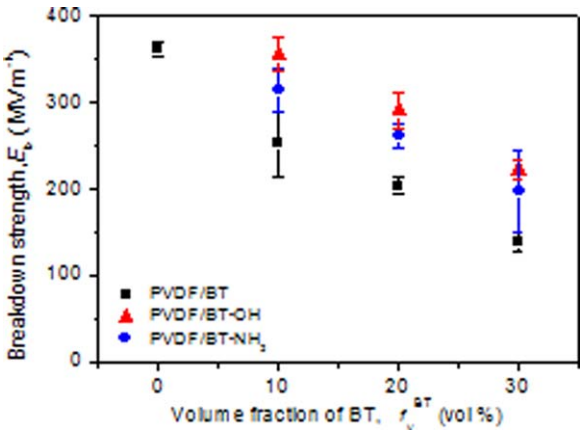

Figure 6. E_b of the pure PVDF and PVDF nanocomposite films with various contents of the raw or modified BT nanoparticles. [Color figure can be viewed in the online issue, which is available at wileyonlinelibrary.com.]

distribution. The vertical gradient distribution of fillers was also observed in BT/PS nanocomposites and BT/PI nanocomposites.[14,22] Besides, the discrepancy between the upper and lower surfaces is also less remarkable. All these results can be explained by the stronger interaction between the modified fillers and the polymer matrix than that between the raw fillers and the polymer matrix. The comparison between Figure 3(a,b) also shows that the nanocomposite films with hydroxylated fillers shows less vertical gradient and less discrepancy between the two surfaces than the nanocomposite films with aminated fillers, which can be explained by stronger interaction between hydroxylated fillers and polymer matrix than that between aminated fillers and polymer matrix. After the chemical modification (hydroxylation and amination), some chemical groups are produced on the surface of filler nanoparticles, which helps separate these nanoparticles. As a result, both the agglomeration and the sedimentation of the fillers are reduced. The more effective anti-agglomeration and anti-sedimenation by BT-OH nanoparticles than by BT-NH_2 might be due to the lower amount of hydrogen bonds formed between BT-OH nanoparticles and PVDF matrix than between BT-NH_2 and PVDF matrix. Therefore, a strong interfacial interaction in this work is formed between BT and PVDF when the BT-OH modification nanoparticles are dispersed into PVDF. This strong interaction makes the BT-OH nanoparticles a better dispersion and prevents the sedimentation of BT-OH nanoparticles during solution casting. However, the BT-NH2 nanoparticles make a poor contribution to these questions, which may be from the loss of –NH2 during the modification.

Figure 4 shows the frequency dependence of dielectric constant (ε) and loss tangent (tan δ) of the pure PVDF, raw BT/PVDF nanocomposite films, and modified BT/PVDF nanocomposite films. From Figure 4(a), it can be seen that the ε increases with increasing content of fillers. Moreover, for the same content of fillers the ε increases in the order of BT-OH > BT-NH_2 > BT. It is a normal phenomenon that the addition of high-ε fillers into a polymer matrix could increase the ε of the latter. This is because the BT fillers with a dielectric permittivity of about 1000, which is one hundred fold higher than PVDF with a permittivity of about 10. In addition, It is interesting to see that the ε of the BT/PVDF nanocomposite films is significantly increased by chemically modifying the BT fillers. It is generally believed that the interfaces between the fillers and matrix is a main reason for the lower ε than expected for the high-ε fillers filled polymer nanocomposite films.[31,32] The chemical modification of BT nanoparticles to BT-OH and BT-NH_2 nanoparticles could increase the interaction between fillers and polymer matrix, which are valuable to polarization between inorganic phase and polymer phase. Therefore, the ε of BT-OH/PVDF and BT-NH_2/PVDF nanoparticle films is higher than that of BT/PVDF nanoparticles. The ε of BT-OH/PVDF nanoparticle films is even higher than that of BT-NH_2/PVDF nanoparticle films probably due to the formation of stronger hydrogen bonds in the former. From Figure 4(b), it can be seen that the evolution of tan δ with the addition of different fillers is complex and dependent on frequency. It is noteworthy that the addition of 10 vol % BT-OH or BT-NH_2 hardly increases the tan δ, especially for the low frequency below 10^5 Hz.

Figure 5 presents the DSC curves of the pure PVDF, raw-BT/PVDF nanocomposite films, and modified-BT/PVDF nanocomposite films. It can be seen that both the crystallization and melting peaks shift to lower temperature with increasing content of fillers. This means that the addition of fillers hinders the crystallization of polymer matrix, which was also observed in the literature.[33] For the same f_v^{BT} of 10 vol %, the melt crystallization temperature (T_{mc}) follows the order: BT-OH/PVDF > BT-NH_2/PVDF > BT/PVDF and the melt crystallization enthalpy (ΔH_{mc}) also follows this order except that the difference between the former two are small. At this f_v^{BT}, the melting temperature (T_m) follows the order: BT-NH_2/PVDF < BT-OH/PVDF < BT/PVDF, while the melting enthalpy (ΔH_m) follows the opposite one. For the same f_v^{BT} of 30 vol %, a similar trend is found except that the difference among three different nanocomposite films becomes much smaller. All these results show that the chemical modification of BT nanoparticles does change the crystallization kinetics because of changes in interaction between the fillers and polymer matrix.

Figure 6 shows the breakdown strength (E_b) of pure PVDF, raw-BT/PVDF nanocomposites, and modified-BT/PVDF nanocomposites. It can be seen that the E_b decreases with increasing f_v^{BT}. For the same f_v^{BT}, the E_b follows the order: BT-OH/PVDF > BT-NH_2/PVDF > BT/PVDF. Compared with pure PVDF films, the addition of BT nanoparticles into polymer matrix decreases E_b because of the formation of defects at the interface between the fillers and matrix.[19,22] The order of E_b, namely, BT-OH/PVDF > BT-NH_2/PVDF > BT/PVDF can be explained by the formation of stronger hydrogen bonds between BT-OH and PVDF than those between BT-NH_2 and PVDF.

CONCLUSION

The effect of the surface modification of BT nanoparticles on their sedimentation in BT/PVDF films during solution casting has been systematically investigated. The surface of BT nanoparticles was hydroxylated by H_2O_2 or aminated by γ-APS. It has been found that the compatibility between fillers and polymer matrix is remarkably improved by such surface treatments. As a

result, the agglomeration and sedimentation in the composites were significantly reduced, as supported by the morphology observation. Better dielectric properties such as higher dielectric constant, higher breakdown strength, and lower dielectric loss are also obtained for the composites with surface-modified fillers than those with raw fillers. Hydroxylated fillers show a better effect than aminated ones.

ACKNOWLEDGMENTS

This work was financially supported by the National Basic Research Program of China (973 Program, Grant No. 2015CB654603) and NSF of China (No.51425201 and 51377010). The authors also acknowledge Ms. Min Chen of University of Science and Technology Beijing for her kind help during manuscript preparation and submission.

REFERENCES

1. Liu, S. H.; Zhai, J. W. *J. Mater. Chem. A* **2015**, *3*, 1511.
2. Arvidson, S. A.; Roskov, K. E.; Patel, J. J.; Spontak, R. J.; Khan, S. A.; Gorga, R. E. *Macromolecules* **2012**, *45*, 913.
3. Urbaniak-Domagala, W. *J. Appl. Polym. Sci.* **2011**, *122*, 2071.
4. Yang, L.; Liu, F.; Xia, H.; Qian, X.; Shen, K.; Zhang, J. *Carbon* **2011**, *49*, 3274.
5. Liu, Y.; Du, B.; Du, D. *Int. Transa. Electr. Energ. Sys.* **2013**, *23*, 72.
6. Lau, K.; Vaughan, A.; Chen, G.; Hosier, I.; Holt, A. *J. Phys. D: Appl. Phys.* **2013**, *46*, 095303-095303-9.
7. Crippa, M.; Bianchi, A.; Cristofori, D.; D'Arienzo, M.; Merletti, F.; Morazzoni, F.; Scotti, R.; Simonutti, R. *J. Mater. Chem. C* **2013**, *1*, 484.
8. Xie, L.; Huang, X.; Wu, C.; Jiang, P. *J. Mater. Chem.* **2011**, *21*, 5897.
9. Kobayashi, Y.; Kurosawa, A.; Nagao, D.; Konno, M. *Polym. Eng. Sci.* **2009**, *49*, 1069.
10. Thomas, P.; Satapathv, S.; Dwarakanath, K.; Varma, K. B. R. *Exp. Polym. Lett.* **2010**, *10*, 632.
11. Siddabattuni, S.; Schuman, T. P.; Dogan, F. *Mater. Sci. Eng.: B* **2011**, *176*, 1422.
12. Chen, F.; Bera, D.; Banerjee, S.; Agarwal, S. *Polym. Adv. Technol.* **2012**, *23*, 951.
13. Luong, N. D.; Hippi, U.; Korhonen, J. T.; Soininen, A. J.; Ruokolainen, J.; Johansson, L.-S.; Nam, J.-D.; Sinh, L. H.; Seppala, J. *Polymer* **2011**, *52*, 5237.
14. Yu, K.; Wang, H.; Zhou,; Y.; Bai, Y.; Niu, Y. *J. Appl. Phys.* **2013**, *113*, 034105-1-7.
15. Zhou, T.; Zha, J. W.; Hou, Y.; Wang, D. R.; Zhao, J.; Dang, Z. M. *ACS Appl. Mater. Interface.* **2011**, *3*, 4557.
16. Dang, Z. M.; Yuan, J. K.; Zha, J. W.; Zhou, T.; Li, S. T.; Hu, G. H. *Prog. Mater. Sci.* **2012**, *57*, 660.
17. Elzayat, M. Y. F.; El-Sayed, S.; Osman, H. M.; Amin, M. *Polym. Eng. Sci.* **2012**, *52*, 1945.
18. Fan, B. H.; Zha, J. W.; Wang, D.; Zhao, J.; Dang, Z. M. *Appl. Phys. Lett.* **2012**, *100*, 012903-012903-4.
19. Fan, P.; Wang, L.; Yang, J.; Zhong, M. *Nanotechnology* **2012**, *23*, 365702.
20. Jung, H. M.; Kang, J. H.; Yang, S. Y.; Won, J. C.; Kim, Y. S. *Chem. Mater.* **2010**, *22*, 450.
21. Yuan, J. K.; Yao, S. H.; Li, W. L.; Sylvestre, A.; Bai, J. B. *J. Phys. Chem. C* **2014**, *118*, 22975.
22. Rock, D. M.; Tan, X. L.; Bowler, N.; Kessler, M. R. Annual Report Conference on Electrical Insulation and Dielectric Phenomena (CEIDP). IEEE Conference on Electrical Insulation and Dielectric Phenomena (CEIDP), Montreal (Canada). **2012**, 912–915.
23. Kuang, D.; Li, R.; Pei, J. *Polymers* **2014**, *6*, 2146.
24. Raihan, R.; Adkins, J.; Baker, J.; Rabbi, F.; Reifsnider, K. *Compos. Sci. Technol.* **2014**, *105*, 160.
25. Wang, D. R.; Bao, Y. R.; Zha, J. W.; Zhao, J.; Dang, Z. M.; Hu, G. H. *ACS Appl. Mater. Interface.* **2012**, *4*, 6273.
26. Lim, S. H.; Zeng, K.; He, C. *Int. J. Mod. Phys. B* **2010**, *24*, 136.
27. Zhou, T.; Zha, J. W.; Cui, R. Y.; Fan, B. H.; Yuan, J. K.; Dang, Z. M. *ACS Appl. Mater. Interface.* **2011**, *3*, 2184.
28. Tang, H.; Ma, Z.; Zhong, J.; Yang, J.; Zhao, R.; Liu, X. *Colloid Surface A: Physicochem. Eng. Aspect.* **2011**, *384*, 311.
29. Zhang, P. Y.; Yang, H.; Xu, Z. L. *Ind. Eng. Chem. Res.* **2012**, *51*, 4388.
30. Li, Y.; Huang, X. Z.; Hu, P.; Jiang, S.; Li, T.; Tanaka, T. *ACS Appl. Meter. Interface.* **2011**, *3*, 4396.
31. Shang, J.; Zhang, Y.; Yu, L.; Luan, X.; Shen, B.; Zhang, Z.; Lva, F. *J. Mater. Chem. A* **2013**, *1*, 884.
32. Liao, W. H.; Yang, S. Y.; Hsiao, S. T.; Wang, Y. S.; Li, S. M. *ACS Appl. Mater. Interface.* **2014**, *6*, 15802.
33. Yang, K.; Huang, X.; Xie, L.; Wu, C.; Jiang, P.; Tanaka, T. *Macromol. Rapid Commun.* **2012**, *33*, 1921.